Polymer 50 (2009) 4199–4204

Contents lists available at ScienceDirect

Polymer

journal homepage: www.elsevier.com/locate/polymer

C_{60} fullerene inclusions in low-molecular-weight polystyrene–poly(dimethylsiloxane) diblock copolymers

Judith H. Waller [a,1], David G. Bucknall [b,*], Richard A. Register [c], Haskell W. Beckham [b], Johannes Leisen [b], Katie Campbell [b]

[a] Dept of Materials, University of Oxford, Oxford OX1 3PH, UK
[b] Polymer, Textile and Fiber Engineering, Georgia Institute of Technology, Atlanta, GA 30332, USA
[c] Chemical Engineering, Princeton University, Princeton, NJ 08544, USA

ARTICLE INFO

Article history:
Received 4 April 2009
Received in revised form
8 June 2009
Accepted 11 June 2009
Available online 30 June 2009

Keywords:
Copolymer
Fullerene
Blend

ABSTRACT

We have synthesized low-molecular-weight diblock copolymers of polystyrene-*block*-poly(dimethylsiloxane) with total molecular weights <12 kg/mol and PS volume fractions of ~0.2. We have investigated the phase behavior of the PS-PDMS in its pure state and with up to 10 wt% of C_{60} added. The C_{60} was shown to selectively segregate into the PS phase only although its solubility limit is ~1 wt%. Although the C_{60} aggregates above 1 wt%, the cylindrical morphology observed in the pure copolymer bulk samples persists in the C_{60}-copolymer composites even up to 10 wt% C_{60} loading. In thin films, the pure copolymer possesses a highly ordered morphology with grains hundreds of microns across. When C_{60} is blended with the copolymer the high degree of order rapidly decreases due to increasing numbers of defects observed.

1. Introduction

Incorporation of fullerenes with polymers often produces dramatic improvements to the polymer properties [1,2] including gas barrier properties [3], microhardness of films [4,5], inhibition of thermo-oxidative degradation [6], photovoltaic efficiency in solar cell applications [7–13], and electro- and photoluminescence [14,15]. However, in most cases, the limited solubility and miscibility of fullerenes in both solvents and polymers [16], coupled with a lack of understanding of how to control these interactions is often a severe restriction to the general utility and wider applicability of using fullerenes. Therefore a majority of studies of polymer–fullerene systems have concentrated on covalently bonding the C_{60} onto the polymer chains thereby avoiding the problems associated with limited solubility [17–23]. Whilst considerable synthetic capability is required to obtain C_{60}-functionalized polymers, simple blending of unfunctionalized fullerenes, in particular C_{60}, with homopolymers has also shown significant modification of a number of the polymer properties including photoluminescence [23,24], heat capacity [25], thin film dewetting behavior [26,27], permeability [28], and thermal stability [29,30]. Functionalization of the fullerene cage, such as [6]-phenyl C_{61} butyric acid methyl ester (PCBM), which is widely utilized for solubilizing C_{60} with a range of conjugated polymers, has been extensively used for incorporating the fullerenes into macromolecular structures [31]. For a recent review of polymers containing fullerenes, see reference [2].

The incorporation of fullerene molecules into block copolymers has been much less widely reported than for metallic or ceramic nanoparticles [32,33]. Due to their limited solubility in most polymers [34,35], functionalization of the fullerene by grafting polymer brushes to the C_{60} cage can promote preferential miscibility of the fullerene into only one block of a diblock copolymer [36–39]. However, this approach adds unnecessary complexity to fullerene synthesis, detracting from the general applicability of using much more widely available unmodified C_{60}. In systems without functionalized fullerenes, hydrogen bonding and acid-base interactions have been used to enhance incorporation of fullerenes into polymers [40,41]. For example, when C_{60} fullerene was added to a PS-P4VP block copolymer, a cylindrical to spherical morphology was induced [42]. In this case, the morphology change was attributed to the electron-accepting C_{60} forming charge-transfer complexes with electron-donating pyridine groups from different P4VP chains [10,42,43]. Despite these studies there remains a limited understanding of polymer–fullerene miscibility and indeed no tool for its prediction.

We are currently investigating inclusion of fullerenes in block copolymers as part of a wider effort to investigate materials for

* Corresponding author.
E-mail address: bucknall@gatech.edu (D.G. Bucknall).
[1] Present address: Laboratory of Composite and Polymer Technology, Ecole Polytechnique Federale de Lausanne, CH-1015 Lausanne, Switzerland.

0032-3861/$ – see front matter © 2009 Elsevier Ltd. All rights reserved.
doi:10.1016/j.polymer.2009.06.060

global quantum information processing (QIP) [44]. In this paper, we discuss the potential use of low-molecular-weight block copolymers as templates for ordering C_{60} fullerenes into cylindrical domains of the block copolymer. The use of low-molecular weight polymers are essential for the length scales of fullerene ordering required for the functionality of the QIP materials.

2. Experimental

Polystyrene-*b*-poly(dimethylsiloxane) (PS-PDMS) diblock copolymers were synthesized by sequential anionic polymerization of styrene and hexamethylcyclotrisiloxane (HMCTS) [45–47]. Cyclohexane and tetrahydrofuran (THF) were distilled from diphenylhexyllithium and sodium benzophenone, respectively, and styrene monomer was purified by distilling from dibutylmagnesium. Polymerizations were performed at room temperature under a nitrogen atmosphere in an Innovative Technologies glovebox (<1 ppm O_2 and H_2O). The polystyrene block was polymerized in cyclohexane containing 0.5 vol% THF, using *sec*-butyllithium initiator. The PS polymerization proceeded for 1 h, following which an aliquot was removed for PS block characterization. To the remaining solution, a small volume of HMCTS in THF was added to allow the crossover to the PDMS polymerization, visually evident by the disappearance of the orange color of the polystyryl anion. At this point, the remaining HMCTS and sufficient THF to produce a roughly 1:1 v/v cyclohexane:THF mixture were added and the reaction vessel was then left stirring continuously for several hours (depending on the molecular weight required) after which point the polymerization was terminated by the addition of a 10-fold excess of chlorotrimethylsilane. Additional details of the synthesis are given elsewhere [45,48].

The molecular weight of the PS block of the copolymers was determined by GPC using Polymer Laboratories PLgel Mixed-C columns and a Waters 410 differential refractive index detector, which was calibrated using a set of narrow molecular weight distribution polystyrene standards. The total molecular weights of the copolymers were determined from peak area analysis using ^{1}H NMR measurements conducted on dilute solutions (0.1 wt%) of the copolymer in deuterated chloroform.

All PS and PS-PDMS samples with and without C_{60} (Fluka, 97% purity) were prepared by rapid precipitation of dilute solutions in toluene (<2 mg/ml) into rapidly stirred cold methanol, followed by filtering and vacuum drying. Free-standing films for SAXS measurements were prepared by pressing the dried powder into 6-mm diameter, 0.75-mm deep PTFE molds and heating at 50 °C for 24 h in a laminar-flow cabinet. Samples for solid-state NMR and WAXS were prepared from the filtered and vacuum-dried precipitate and measured in a ceramic 4-mm MAS rotor (NMR) or 1-mm capillary tubes (WAXS). Samples for TEM were prepared by adding 1 drop of the 0.5 wt% copolymer solution onto the surface of stirred distilled water heated to 90 °C. The resulting film was then picked up from the surface of the water onto 200 mesh Cu TEM grids (Agar Scientific, UK).

TEM images were collected using a JEOL 2000FX microscope operated at 100 keV. X-ray data collection from the copolymers and composites were carried out using a Bruker AXS NanoSTAR for SAXS measurements and a Rigaku MicroMax 002 with R-axis IV++ detector for WAXS measurements. Both X-ray systems used Cu anodes operated at 40 kV and 35 mA.

Solid-state NMR spectra were recorded on a Bruker DSX-400 solid-state NMR spectrometer operating at a magnetic field strength of 9.4 T. The samples were measured at 0 °C at a magic-angle spin speed of 5 kHz. Spin-diffusion experiments were conducted with a ^{1}H dipolar filter sequence followed by a mixing time (t_m) and then cross-polarization (CP) for measurement of ^{13}C NMR spectra [49,50]. The ^{1}H and ^{13}C 90° pulse durations were set to 5 μs. The dipolar filter consisted of two 12-pulse cycles in which each pulse was separated by a 30-μs duration. The contact time for magnetization transfer from ^{1}H to ^{13}C was 2 ms. All ^{13}C data were recorded under conditions of ^{1}H broadband decoupling during an acquisition time of 12.338 ms (1024 complex data points with a 12-μs dwell time). For the spin-diffusion experiment, 6000 scans were recorded for five different mixing times from 0.5 to 500 ms and the average peak areas normalized against those measured at the longest t_m (500 ms).

3. Results and discussion

Two different PS-PDMS copolymers were synthesized with molecular characteristics as shown in Table 1. The molecular weights of the PS blocks of the copolymers were determined using GPC on an aliquot of PS extracted from the reaction mixtures before HMCTS was added. The molecular weight of the PDMS blocks were determined from solution NMR measurements of the molar ratio of PDMS to PS using the methyl protons for the PDMS and the aromatic protons for the PS. These NMR-determined mole fractions were used to determine the corresponding weight fractions of PS in the copolymers. The polydispersities of the copolymers were determined by GPC. The increase in the polydispersities of the copolymers compared to those of the PS blocks is attributed to competing depolymerization of the PDMS units to form small cyclics, especially the cyclic tetramer. This increase in polydispersity effectively limited the reaction time and therefore the total PDMS block length able to be grown without significantly increasing its polydispersity. An additional contribution to the apparent polydispersity was a shoulder to the major copolymer elution peak observed in the GPC trace, which is associated with homo-PDMS impurity. Methods of removing homo-PDMS from these copolymers have been discussed by Chu et al. [45], however, since the levels of impurity were calculated to be approximately 2 wt%, the copolymers were not purified further.

The location of the C_{60} in the microphase-separated copolymers was determined using solid-state NMR spin-diffusion [49,50]. Following excitation of all of the protons in the sample, the rigid-phase ^{1}H signal (i.e., from PS) was destroyed using a dipolar filter. The remaining magnetization (i.e., PDMS) was then allowed to "diffuse" through the sample for variable mixing times until equilibrium was reached. The spin-diffusion progress was monitored by transferring the ^{1}H signal to the ^{13}C nuclei via cross-polarization (CP) before detection. Since the C_{60} contains no attached protons and must therefore polarize from those in its immediate neighborhood, its location was monitored by comparing its polarization rate with that of the similarly non-protonated carbons of the PS phenyl side groups. Consequently, C_{60} contained within the PS phase would polarize at comparable rates as these non-protonated PS carbons. However, any C_{60} located at the PS-PDMS interface or in the PDMS phase, would cause the C_{60} signal to appear more rapidly.

Table 1
PS-PDMS copolymer characteristics.

Copolymer code	Weight fraction w_{PS}	M_n (PS) g/mol[a]	M_w/M_n (PS)	M_w/M_n (PS-PDMS)[a]	M_n (PDMS) g/mol[b]	T_{ODT} (°C)[c]
S3	0.235	2200	1.07	1.22	7200	139 ± 1 °C
S4	0.174	2100	1.07	1.21	10,000	97 ± 1 °C

[a] Determined from GPC measurements calibrated against PS standards.
[b] Calculated based on solution NMR measurements of the molar ratio of PDMS to PS.
[c] Determined from temperature dependent SAXS measurements of abrupt primary diffraction peak broadening using a SAXS system consisting of an Anton Paar compact Kratky camera, a Braun 1-D position-sensitive detector, and a custom-built hot-stage.

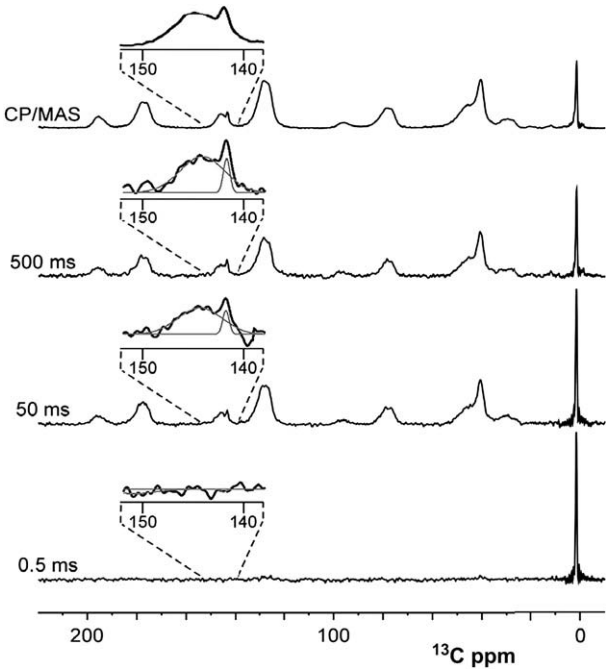

Fig. 1. ^{13}C solid-state NMR spectra of a solution-blended composite of C_{60} with the S3 (3 wt% C_{60}) diblock copolymer measured at 0 °C and while magic-angle spinning (MAS) at 5 kHz. The standard cross-polarization (CP) MAS spectrum is shown at the top. The other three spectra are the ^{13}C CP/MAS spectra measured after destruction of the rigid-phase magnetization and then spin diffusion for the mixing times indicated on each: 0.5, 50 and 500 ms. The insets show the region between 140 and 150 ppm, which contains the peaks due to the C_{60} (142 ppm) and the non-protonated phenyl carbons of the PS (145 ppm).

A standard CP/MAS solid-state ^{13}C NMR spectrum of the solution-blended sample of 3 wt% C_{60} in the S3 copolymer is shown in Fig. 1. A single sharp peak near 0 ppm is due to the PDMS. The PS peaks are broader, reflecting less mobility, and appear at 38–51 ppm for the backbone methylene and methine carbons, around 129 ppm for the side-group protonated phenyl carbons, and at 145 ppm for the non-protonated phenyl carbons [51]. The C_{60} peak appears at 142 ppm [52] and overlaps with the peak due to the non-protonated carbons of the PS phenyl groups. This region is shown expanded in the insets of Fig. 1. In the full CP/MAS spectrum, sets of spinning side bands appear 5 kHz (50 ppm) downfield (179/195 ppm) and upfield (79/95 ppm) from the aromatic PS carbon peaks. The small peak near 29 ppm is also a spinning side band from the protonated aromatic PS carbons.

Following application of the dipolar filter, none of the PS or C_{60} peaks appear in the ^{13}C spectrum. This is shown in Fig. 1 in the spectrum collected after a very short mixing time of 0.5 ms. The expanded inset shows no signal for the C_{60} or the non-protonated PS carbons from 140 to 150 ppm. This result indicates that C_{60} is not located in the PDMS phase. If it were, its ^{13}C peak would appear along with the PDMS ^{13}C peak via cross-polarization from the selected ^{1}H magnetization of the PDMS. To confirm this, the peak intensity versus mixing times needs to be evaluated. For mixing times longer than 0.5 ms, the PS and C_{60} peaks appear and grow at the expense of the PDMS peak. For each mixing time, the overlapping C_{60} and non-protonated PS phenyl peaks were deconvolved by fitting. The Gaussian line shapes used for fitting can be seen in the expanded insets for the spectra collected with 50 and 500 ms mixing times. Average peak areas from two separate spin-diffusion data sets are shown in Fig. 2 as a function of the square root of the mixing time, $\sqrt{t_m}$. The data in Fig. 2 have been normalized to peak areas at the longest t_m (500 ms) and the solid line is an exponential

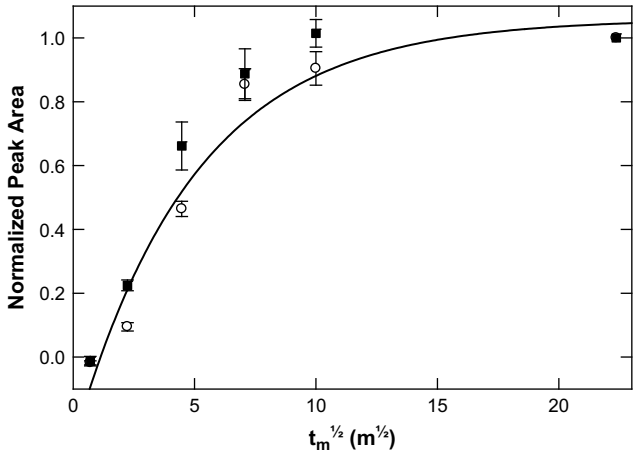

Fig. 2. ^{13}C solid-state NMR peak area versus the square root of the spin-diffusion mixing time, $(t_m)^{1/2}$, for the non-protonated carbon of the PS phenyl side groups (■) and the C_{60} (○) in the S3:C_{60} blend (3 wt% C_{60}). These NMR peak areas are normalized to the areas at $t_m = 500$ ms, and are the averages of two separate experiments. The solid line is an exponential fit to the data.

fit to the data. The C_{60} and the non-protonated phenyl carbons of the PS polarize at very similar rates, meaning that the C_{60} is only found within the PS phase of the copolymer.

Once it was established that the C_{60} was found only in the PS phase of the copolymer, we evaluated the solubility limit of C_{60} in PS using WAXS measurements. The WAXS patterns for all the PS samples clearly show 3 broad peaks centered at $2\theta = 10.1$, 19.6 and 42.5°, which are characteristic of amorphous PS scattering (see Fig. 3). The PS-C_{60} blends with ≥2 wt% C_{60} also show distinct diffraction peaks, which are consistent with the peaks from pure C_{60}. Even at 1 wt% addition of C_{60}, weak fullerene peaks do appear as shoulders to the amorphous scattering peaks of the PS at $2\theta = 17.8$ and 20.9°. Clearly even at these low weight fractions, not all the fullerene is fully solubilized by the PS. Since no C_{60} diffraction peaks are visible in the 0.5 wt% sample, we estimate that the solubility limit of C_{60} in PS to close to 1 wt%, given the fullerene diffraction peaks are only just visible at this concentration. This result is consistent with molecular dynamic (MD) modeling results, which estimates the thermodynamic solubility limit of C_{60} in PS to be 1.6 wt% [53]. The differences in these experimental and theoretical values are acceptable given the inherent assumptions built into the MD calculations.

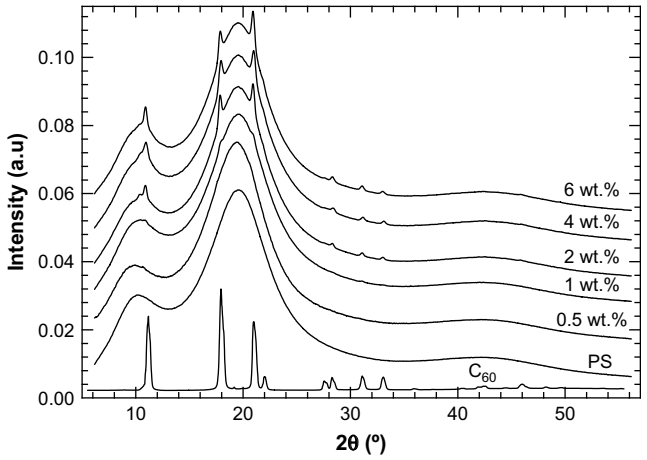

Fig. 3. WAXS diffraction patterns from C_{60}, PS and PS with increasing weight fractions of C_{60} added (as indicated). Data have been scaled for clarity.

The effect of the presence of C_{60} inclusions on the copolymer morphology was evaluated using SAXS and TEM. The radially averaged SAXS patterns for the pure S3 and S4 copolymers show distinct primary peaks at $Q_1 = 0.495 \pm 0.002$ and $0.493 \pm 0.002\ nm^{-1}$, respectively, which are both equivalent to a characteristic dimension of $L = 12.7 \pm 0.1$ nm. The similarity in dimension of these two copolymers results from a fortuitous combination of differences in total molecular weight and compositions. Both copolymers exhibit a weaker secondary peak at a relative peak position of $\sqrt{3}\cdot Q_1$. These peak positions are consistent with cylindrical (hexagonal) copolyxmer morphology, which is expected based on volume fraction considerations. On close examination of the S4 data at the position of the expected third order peak (at $\sqrt{4}\cdot Q_1$) a very weak maximum is observed, although the data in this region are very noisy so this peak cannot be confirmed unambiguously. Gyroid or other less common structures cannot be ruled out from these SAXS data, but from analysis of the TEM data these structures were later discounted. The lack of higher order peaks is simply associated with the short-range order of the copolymer domains in these bulk samples.

SAXS data for the S4-C_{60} composite samples as a function of increasing fullerene content are shown in Fig. 4. As was seen for the pure S4 copolymer, the composite samples also have a clear primary peak at Q_1 ($0.493 \pm 0.002\ nm^{-1}$), with weaker peaks at $\sqrt{3}Q_1$ and $\sqrt{4}Q_1$ and no peak at $\sqrt{2}Q_1$ indicating a hexagonal (cylindrical) phase morphology. Similar behavior is also observed with the S3-C_{60} composites. When C_{60} is blended with the copolymers, perhaps surprisingly, not only is the cylindrical morphology retained but the characteristic dimensions are also unchanged (the primary peak does not change its Q position) even at the highest weight fractions of C_{60}. However, this is not as surprising as may initially be thought since the amount of C_{60} present is still relatively low, so there are going to be large volumes of copolymer between individual fullerenes (or clusters) which are largely unaffected by the presence of the particles.

Although the cylindrical morphology is retained, the aggregation of the fullerenes with increasing concentration produces increasing amounts of excess scattering for C_{60} contents of >1 wt%, i.e., above the C_{60} solubility limit. The excess scattering occurs at medium and low Q values, *i.e.*, at approximately $Q < 0.8\ nm^{-1}$, equivalent to length scales of ~8 nm or greater. At $Q < 0.4\ nm^{-1}$, equivalent to length scales of ~16 nm or greater, the excess scattering has to be due to correlations between long-range density fluctuations that are larger than the characteristic cylinder repeat distance of the copolymer. Quantification of the excess scattering through determination of the scattering invariant [54] indicates that there is little change in the structure of both S3 and S4 copolymers until loadings of $C_{60} \geq 2$ wt% are exceeded. This suggests that below these levels of loading even though fullerenes are clustering, the mean diameters of these aggregates remain small and the copolymer is largely able to accommodate them within the cylindrical PS phase without significant changes to its morphology. As the weight fraction of C_{60} increases the cluster size becomes significant and this ultimately affects the longer range domain morphology of the copolymer by the introduction of defects.

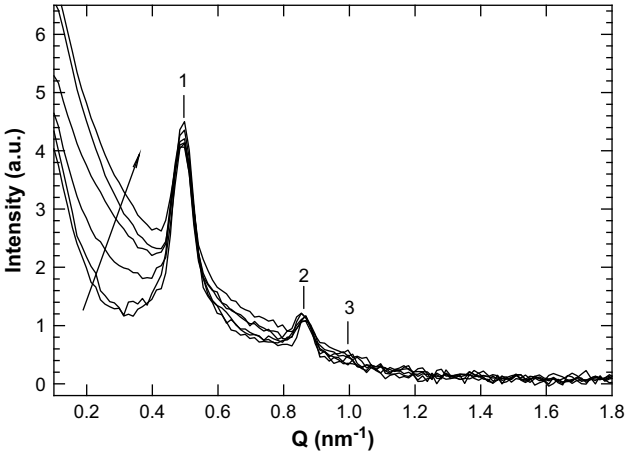

Fig. 4. SAXS patterns for the S4 copolymer as a function of wt% C_{60} added (with respect to PS content). The arrow indicates an increasing concentration of C_{60}: 0, 1, 2, 3, 5 and 7.5 wt%. The diffraction peaks indicated (1, 2 and 3) are the primary peak, Q_1 at 0.495 nm-1, a secondary peak at $Q = \sqrt{3}\cdot Q_1$, and evidence of a weak tertiary peak at $\sqrt{4}\cdot Q_1$, which is consistent with hexagonal ordering (see text).

Changes to the width of the primary peak (Q_1) were used to determine the variation in average copolymer characteristic dimension with increasing weight fraction of C_{60}. For S4 there is no discernable change in width of the primary peak, indicating that the C_{60} does not affect the average size of the copolymer domains. These data clearly indicate that the local phase morphology of the copolymer is therefore largely unperturbed by the addition of increasing weight fractions of C_{60}. For the S3 composites, the primary peak width is essentially constant below 3 wt% C_{60}, but increases at concentrations higher than this. This indicates that above 3 wt% there is an increase in the size distribution of the characteristic dimensions, that is to say, the PS phase cylindrical diameter increasingly varies along its long axis with increasing C_{60} content as the copolymer deforms around the fullerene particles [55]. However, since the primary peak position remains constant, clearly the average characteristic dimension of the copolymer is not varying for either copolymer with increasing fullerene loading.

The scattering results are also largely confirmed by analysis of the TEM micrographs for the C_{60} composite films, although care needs to be taken in making exact comparisons with the SAXS results since the samples were prepared in different ways. The TEM films of pure S3 copolymer demonstrate a very remarkable degree of domain ordering, forming a highly linear and near defect-free morphology (see Fig. 5). The ordering in the thin films persists over a long range, well beyond the scan size of the image. Indeed, unlike most copolymer films no grain boundaries are observed and the domains maintain the same order director beyond the 200 × 200 μm area that was able to be surveyed using the TEM stage [48]. A similar degree of domain regularity is also observed for the pure S4 copolymer films. Numerous samples of both pure S3 and S4 were examined by TEM, and remarkably few defects were observed. Where defects were seen, they comprised almost entirely of dislocations, and thus the directional orientation of the sample was conserved over the whole area.

The significant degree of order in these pure copolymer films is assumed to result from the mobility of the PDMS segments (T_g in the bulk is −120 °C) coupled with the short chain lengths ($N_{total} = 118$ for S3), which allow the chains to eliminate defects when the films are being formed. The elevated temperatures used during film formation (90 °C) in the pure copolymers are clearly playing a role in promoting defect annihilation, since the PS at this molecular weight (~2 kg/mol) is well above its T_g. The kinetics of this defect annihilation and development of order is extremely rapid compared for example, to PS-poly(ethylene-propylene) films, where ordered samples could only be obtained either by long annealing times of the order of 3 h to produce grains 1 μm^2 or through applying shear to the film [56].

The effect of C_{60} inclusion in S3 and S4 copolymers is very similar, with representative TEM images for S3 shown in Fig. 5. Even for a very modest inclusion of 0.5 wt% C_{60} the near perfect ordering is disrupted with a number of defects observed. An increasing number of defects are observed with increasing C_{60} content. At and above 5 wt% C_{60} content, the microdomain morphology of the copolymer

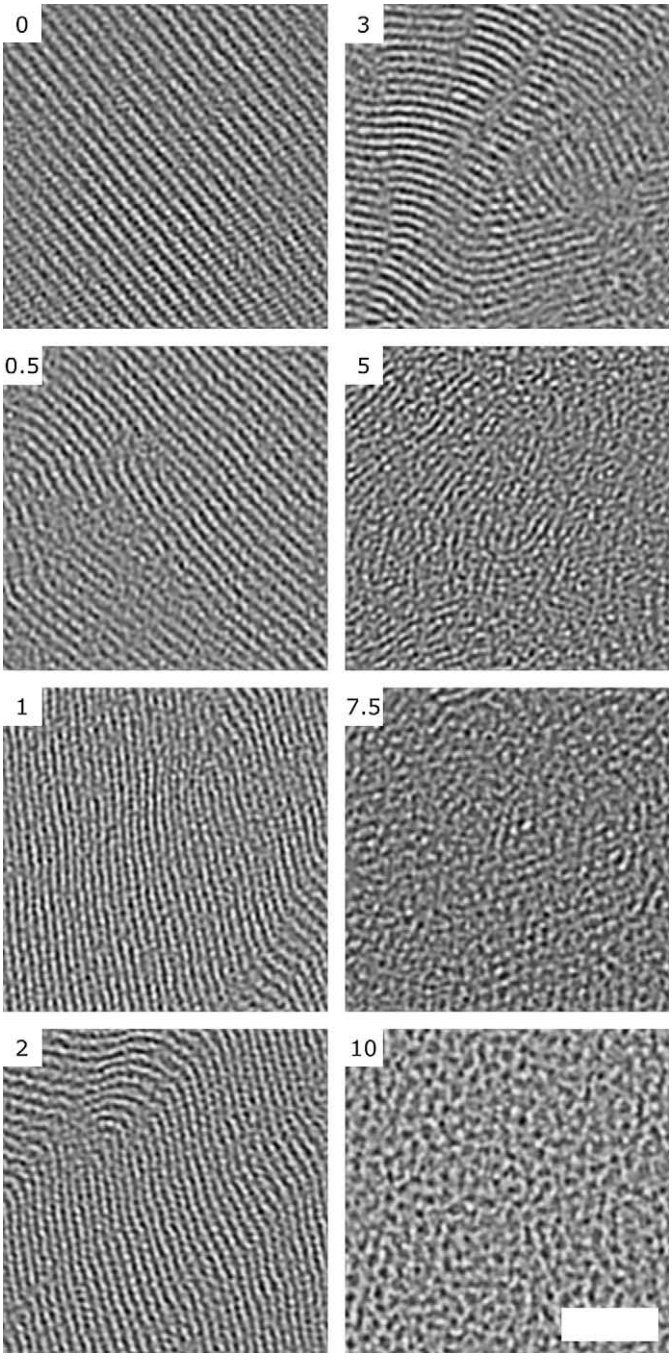

Fig. 5. TEM images of S3 copolymer with various amounts of C_{60}. The number in the top left hand corner of each image indicates the wt% of C_{60}, with respect to PS content; the scale bar corresponds to 100 nm. The addition of C_{60} to the copolymer appears to increase the number of defects in the sample.

becomes significantly more disordered, with significant numbers of defects visible. The TEM data were analyzed for microdomain orientation by determining orthogonal pixel intensity differences to derive the order parameter defined as $\cos(2\Delta\theta)$, where $\Delta\theta$ is the difference between the domain direction and the average orientation of the grain [57]. The order parameters determined for the S3 and S4 samples are given in Table 2, where increasing additions of C_{60} cause the order parameter to decrease.

The SAXS and TEM results qualitatively agree with the work of Huh et al. [58] who determined the theoretical phase behavior of diblock copolymers in the presence of nanoparticles. In the strong segregation limit, they showed that the incompressibility of the system forces stretching of the chains around the nanoparticles, causing the chains to incur an additional free-energy loss. The magnitude of this free energy for any fixed copolymer composition depends on the size of the particle relative to the radius of gyration of the surrounding chains. Therefore, it is expected that addition of nanoparticles to a diblock copolymer with a fixed composition would have the effect of pushing the system towards a more disordered state as the size of the nanoparticles increase. This predicted behavior agrees well with the observed differences between the pure copolymer and C_{60} composite.

Table 2
Order parameters determined from TEM analysis. The order parameter was obtained from computational analysis of the TEM images.

wt. % C_{60}	S3	S4
0	0.73	0.74
0.5	0.67	0.63
1	0.74	0.38
2	0.57	0.03
3	0.48	0.39
5	0.30	0.27
7.5	0.18	0.19
10	0.14	0.27

4. Conclusions

Low-molecular-weight PS-PDMS diblock copolymers have been synthesized with total molecular weights of 9.4 and 12.1 kg/mol and weight fractions of the PS blocks of 0.17 and 0.24. Despite the low-molecular weights of these copolymers, they phase separate to give a cylindrical morphology in the bulk as determined by SAXS, with a PS cylinder repeat spacing of ~13 nm. The morphological behavior of the pure PS-PDMS copolymers and its physical blends with increasing loadings of C_{60} has been investigated. The solubility limit of C_{60} in PS was determined to be ~1 wt%. Using solid-state NMR measurements it has been shown that the C_{60} fullerenes are completely surrounded by PS chains, even when the C_{60} loading (3 wt%) is above its apparent solubility limit in PS and consequently aggregated into clusters.

In thin films, pure copolymers form highly ordered, near defect-free grains which extend over several hundred microns. When C_{60} was included into the copolymer the reduced entropic energy associated with PS chain stretching in the vicinity of the C_{60} fullerene aggregates is balanced by the increase of entropy by the introduction of defects into the copolymer phase morphology. Despite the introduction of defects caused by inclusion of C_{60}, the SAXS results showed that the copolymer system still retains some degree of its cylindrical morphology.

These results indicate that as the C_{60} cluster sizes grow, as evidenced by the increase in excess scattering in the SAXS, the copolymer domains must locally distort around the clusters in order for the fullerenes to remain surrounded by PS chains. In the TEM data even at high C_{60} loadings where larger clusters might be expected, no aggregates are directly observed. This is perhaps not surprising since there is very little natural contrast between the C_{60} and PS given that both are C-rich molecules and both contain aromatic rings.

Acknowledgements

The authors are extremely grateful to Prof Tony Ryan and Dr. S. Mykhaylyk at University of Sheffield for fruitful discussions as well as use of their SAXS equipment, Dr Andrew Watt at University of

Oxford for assisting in the TEM studies, and Mrs B. Gurun for WAXS measurements. We thank Sasha Myers at Princeton University for assistance in the diblock synthesis and characterization. J.H.W. thanks the Oxford-Princeton Partnership and the Princeton Center for Complex Materials, funded by the National Science Foundation (DMR-0213706 and DMR-0819860), for their support of her research at Princeton. This work was additionally supported by the NSF under the Materials World Network program (DMR-0710467).

References

[1] Chichak KS, Star A, Altoe MVR, Stoddart JF. Small 2005;1(4):452–61.
[2] Wang CC, Guo ZX, Fu SK, Wu W, Zhu DB. Progress in Polymer Science 2004; 29(11):1079–141.
[3] Polotskaya GA, Gladchenko SV, Zgonnik VN. Journal of Applied Polymer Science 2002;85(14):2946–51.
[4] Calleja FJB, Giri L, Asano T, Mieno T, Sakurai S, Ohnuma M, et al. Journal of Materials Science 1996;31(19):5153–7.
[5] Lu Z, He C, Chung TS. Polymer 2001;42(12):5233–7.
[6] Troitskii BB, Domrachev GA, Khokhlova LV, Anikina LI. Polymer Science Series A 2001;43(9):964–9.
[7] Yang X, Loos J. Macromolecules 2007;40(5):1353–62.
[8] Kim Y, Choulis SA, Nelson J, Bradley DDC, Cook S, Durrant JR. Journal of Materials Science 2005;40(6):1371–6.
[9] Gunes S, Neugebauer H, Sariciftci NS. Chemical Reviews 2007;107(4):1324–38.
[10] Barber RP, Gomez RD, Herman WN, Romero DB. Organic Electronics 2006;7(6):508–13.
[11] Blom PWM, Mihailetchi VD, Koster LJA, Markov DE. Advanced Materials 2007; 19(12):1551–66.
[12] Segura JL, Martin N, Guldi DM. Chemical Society Reviews 2005;34(1):31–47.
[13] Segura JL, Giacalone F, Gomez R, Martin N, Guldi DM, Luo CP, et al. Materials Science & Engineering C – Biomimetic and Supramolecular Systems 2005; 25(5–8):835–42.
[14] Lee TW, Park OO, Kim J, Kim YC. Macromolecular Research 2002;10(5):278–81.
[15] Kim H, Kim JY, Park SH, Lee K, Jin Y, Kim J, et al. Applied Physics Letters 2005; 86(18):183502.
[16] Hansen CM, Smith AL. Carbon 2004;42(8–9):1591–7.
[17] Weber V, Duval M, Ederle Y, Mathis C. Carbon 1998;36(5–6):839–42.
[18] Janot JM, Eddaoudi H, Seta P, Ederle Y, Mathis C. Chemical Physics Letters 1999;302(1–2):103–7.
[19] Ederle Y, Nuffer R, Mathis C. Synthetic Metals 1999;103(1–3):2348–9.
[20] Wang CC, Pan BR, Fu SK, Jing KJ, Chen HZ, Wang M. Macromolecular Chemistry and Physics 1996;197(11):3783–90.
[21] Aleshin AN, Biryulin YF, Mironkov NB, Sharonova LV, Fadeeva EN, Zgonnik VN. Fullerene Science and Technology 1998;6(3):545–61.
[22] Pantazis D, Pispas S, Hadjichristidis N. Journal of Polymer Science, Part A: Polymer Chemistry 2001;39(14):2494–507.
[23] Li GZ, Minami N, Ichio Y. Polymer Engineering and Science 2001;41(9):1580–8.
[24] Zhang C, Xiao XD, Ge WK, Loy MMT, Wang DZ, Zhang QJ, et al. Applied Physics Letters 1996;68(7):943–5.
[25] Smirnova NN, Markin AV, Boronina IE, Lopatin MA. Thermochimica Acta 2005;433(1–2):121–7.
[26] Barnes KA, Karim A, Douglas JF, Nakatani AI, Gruell H, Amis EJ. Macromolecules 2000;33(11):4177–85.
[27] Barnes KA, Douglas JF, Liu DW, Karim A. Advances in Colloid and Interface Science 2001;94(1–3):83–104.
[28] Gladchenko SV, Polotskaya GA, Gribanov AV, Zgonnik VN. Technical Physics 2002;47(1):102–6.
[29] Shibaev LA, Antonova IA, Vinogradova LV, Ginzburg BM, Zgonnik VN, Melenevskaya EY. Russian Journal of Applied Chemistry 1998;71(5):862–8.
[30] Troitskii BB, Khokhlova LV, Konev AN, Denisova VN, Novikova MA, Lopatin MA. Polymer Science Series A 2004;46(9):951–6.
[31] Wang CC, He JP, Fu SK, Jiang KJ, Cheng HZ, Wang M. Polymer Bulletin 1996;37(3):305–11.
[32] Jenekhe SA, Chen XL. Science 1998;279(5358):1903–7.
[33] Sivula K, Ball ZT, Watanabe N, Frechet JMJ. Advanced Materials 2006;18(2): 206–10.
[34] Okamura H, Terauchi T, Minoda M, Fukuda T, Komatsu K. Macromolecules 1997;30(18):5279–84.
[35] Wang ZY, Kuang L, Meng XS, Gao JP. Macromolecules 1998;31(16):5556–8.
[36] Ederle Y, Mathis C. Macromolecules 1997;30(9):2546–55.
[37] Schmaltz B, Brinkmann M, Mathis C. Macromolecules 2004;37(24):9056–63.
[38] Samulski ET, Desimone JM, Hunt MO, Menceloglu YZ, Jarnagin RC, York GA, et al. Chemistry of Materials 1992;4(6):1153–7.
[39] Ball ZT, Sivula K, Frechet JMJ. Macromolecules 2006;39(1):70–2.
[40] Huang XD, Goh SH, Lee SY. Macromolecular Chemistry and Physics 2000;201(18):2660–5.
[41] Fujita N, Yamashita T, Asai M, Shinkai S. Angewandte Chemie-International Edition 2005;44(8):1257–61.
[42] Laiho A, Ras RHA, Valkama S, Ruokolainen J, Osterbacka R, Ikkala O. Macromolecules 2006;39(22):7648–53.
[43] Chen XL, Jenekhe SA. Langmuir 1999;15(23):8007–17.
[44] Benjamin SC, Ardavan A, Andrew G, Briggs D, Britz DA, Gunlycke D, et al. Journal of Physics-Condensed Matter 2006;18(21):S867–83.
[45] Chu JH, Rangarajan P, Adams JL, Register RA. Polymer 1995;36(8):1569–75.
[46] Zilliox JG, Roovers JEL, Bywater S. Macromolecules 1975;8(5):573–8.
[47] Hartney MA, Novembre AE, Bates FS. Journal of Vacuum Science & Technology B 1985;3(5):1346–51.
[48] Waller JH. The effect of nanoparticle inclusion of diblock copolymer morphology. DPhil thesis, University of Oxford, 2007.
[49] Schmidt-Rohr K, Spiess HW. Multidimensional solid-state NMR and polymers. London: Academic Press; 1994.
[50] Nagapudi K, Leisen J, Beckham HW, Gibson HW. Macromolecules 1999;32(9):3025–33.
[51] Yang H, Kwei TK, Dai Y. Macromolecules 1993;26(4):842–3.
[52] Yannoni CS, Johnson RD, Meijer G, Bethune DS, Salem JR. Journal of Physical Chemistry 1991;95(1):9–10.
[53] Bucknall DG, Unpublished results, 2008.
[54] Roe RJ. Methods of X-ray and neutron scattering in polymer science. New York: Oxford University Press; 2000.
[55] Bockstaller MR, Mickiewicz RA, Thomas EL. Advanced Materials 2005; 17(11):1331–49.
[56] Angelescu DE, Waller JH, Adamson DH, Deshpande P, Chou SY, Register RA, et al. Advanced Materials 2004;16(19):1736–40.
[57] Pelletier V, Adamson DH, Register RA, Chaikin PM. Applied Physics Letters 2007;90(16):163105.
[58] Huh J, Ginzburg VV, Balazs AC. Macromolecules 2000;33(21):8085–96.